PCCP

PAPER

View Article Online
View Journal | View Issue

Cite this: *Phys. Chem. Chem. Phys.*, 2014, **16**, 16039

Uniaxial deformation of nanorod filled polymer nanocomposites: a coarse-grained molecular dynamics simulation†

Yangyang Gao,[ab] Jun Liu,[ab] Jianxiang Shen,[b] Liqun Zhang,*[ab] Zhanhu Guo*[c] and Dapeng Cao*[a]

A coarse-grained molecular dynamics simulation was used to investigate the stress–strain behavior of nanorod-filled polymer composites. The effects of the interfacial interaction, aspect ratio of fillers, filler functionalization, chemical couplings between the polymer and the filler and the filler loading on the mechanical reinforcement were explored. The results indicate that there exists an optimal nanorod volume fraction for elastomer reinforcement. The strong polymer–nanorod interaction enhances the reinforcement of polymer nanocomposites. Meanwhile, it is found that nanorods with longer length and smaller diameter, and the chemical functionalization of nanorods can help realize the efficient interfacial stress transfer. And excessive chemical couplings between polymers and nanorods are harmful to mechanical properties. An upturn in the modulus at large deformation is observed in the Mooney–Rivlin plot, attributed to the limited chain extensibility. Particularly, the medium polymer–nanorod interfacial strength and low nanorod volume loading will lead to better dispersion of nanorods. It is suggested that the reinforcement mechanism comes from the nanorod alignment and bond orientation, as well as from the limited extensibility of chain bridges at large deformation. In addition, an optimal nanorod volume fraction can also be explained by the strong polymer–nanorod network. Compared to glassy systems, the mechanism for the significantly enhanced reinforcement of rubbery systems is also demonstrated. In short, our simulation study of nanorod-induced mechanical reinforcement will provide a basic understanding of polymer reinforcement.

Received 10th April 2014,
Accepted 5th June 2014

DOI: 10.1039/c4cp01555j

www.rsc.org/pccp

1. Introduction

In the field of nanotechnology, polymer matrix based nanocomposites have attracted significant attention. It is well known that the incorporation of nanoscopic fillers (such as carbon black, silica, carbon nanotubes, clay sheets and graphene) in the elastomer matrix can markedly improve its mechanical, electrical and other properties. In fact, a wide variety of fillers are utilized in the rubber industry like carbon black, silica and clay sheets. These fillers have been considered to be the most successful example in the industrial application of polymer nanocomposites. Although the microscopic reinforcing mechanism is not fully understood yet, the effect of fillers on the reinforcement of elastomer is of scientific and commercial importance.

In the literature, the preparation, structure and properties of different polymer nanocomposites (PNCs) were reviewed.[1–3] Currently, a number of theories have been proposed. Because of the introduced rigid filler particles in rubber matrices, the hydrodynamics reinforcement or strain amplification has a contribution to the reinforcement. The simple Einstein–Smallwood formula[4] is proposed based on several assumptions and then some improvements are made by Gold and Guth.[5,6] Huber *et al.*[7] presented a theoretical investigation concerning the hydrodynamics reinforcement contribution using different structural fillers. The "interaction zone" hypothesis claimed that a reduction in polymer mobility near the surface of a particle arises from a local reorganization of the polymer into a more structured or possibly glassy state.[8,9] Another hypothesis was that the fillers may act as highly functional cross-links[10] capable of forming polymer bridges between them. Litvinov *et al.*[11] observed a tightly bound layer, a loosely bound chain and the extractable chains in the case of the carbon black filled ethylene propylene diene monomer (EPDM). Meanwhile, it was found that the

[a] *State Key Laboratory of Organic-Inorganic Composites, Beijing University of Chemical Technology, Beijing 100029, People's Republic of China. E-mail: caodp@mail.buct.edu.cn*
[b] *Key Laboratory of Beijing City on Preparation and Processing of Novel Polymer Materials, Beijing University of Chemical Technology, Beijing 100029, People's Republic of China. E-mail: zhanglq@mail.buct.edu.cn*
[c] *Integrated Composites Laboratory (ICL), Dan F. Smith Department of Chemical Engineering, Lamar University, Beaumont, TX 77710, USA. E-mail: zhanhu.guo@lamar.edu*

† Electronic supplementary information (ESI) available. See DOI: 10.1039/c4cp01555j

introduced nanofillers decrease the number of dangling and free chains.[12] Long *et al.*[13] pointed out that the strong reinforcement can be achieved when glassy layers between fillers overlap. They also showed that the dynamics of yield and rebirth of glassy bridges can account for the nonlinear Payne effect and the Mullins effect. Bokobza *et al.*[14] observed a steep upturn in the Mooney–Rivlin plots in the filled poly(dimethylsiloxane) (PDMS) networks, which was attributed to the limited chain extensibility of the short chains linking filler particles. Especially, a double network model was developed to quantitatively describe the stress–strain behavior.[15]

Many parameters may play a role in reinforcement of the polymer matrix, such as the diameter, length, aspect ratio, surface-functionalization, dispersion state, nanotube loading, and interfacial adhesion.[16] Meanwhile, Coleman *et al.*[17,18] discussed the mechanism for effective reinforcement and proposed a model. It showed that the tensile strength increased in proportion to the thickness of the interface region. Deng *et al.*[19] indicated that the length and reorientation of multiwalled carbon nanotubes during stretch have a significant impact on the mechanical properties. Synergistic weak interactions between carbon-nanotubes (CNTs) grafted with short polymer chains can better enhance the mechanical properties of CNT-based materials.[20] By functionalizing carbon with high bonding density of polymer layers, it exhibited a pronounced effect on the mechanical properties of polystyrene composites.[21] And efficient load transfer to polymer-grafted multiwalled carbon nanotubes was revealed.[22] Through covalent integration of functionalized nanotubes, it enhances the mechanical properties of the epoxy polymer composites.[23] Poly(methyl methacrylate) (PMMA)-functionalized multiwalled carbon nanotubes were prepared to reinforce the PMMA matrix and an optimum filler volume fraction was observed.[24]

In fact, because of various length and time scales,[25] it becomes very complicated to investigate the rubber reinforcement. At low filler loading, the reinforcement mainly comes from the interfacial strength between rubber and fillers, while at high loading, the complicated networks containing rubber–filler and filler–filler will have an effect. So computer simulation studies were employed to elucidate the rubber reinforcement mechanism. The results[26] suggested that the nanorod length does not meaningfully affect the elastic properties of glassy polymer composites but does affect the post-yield properties. The viscosity and isotropic tensile strength of icosahedra, rods, and sheets were examined using a coarse-grained bead-spring model.[27] Ozmusul *et al.*[28] found that the mechanical behavior of nanocomposites results from the formation of a long-lived transient filler network mediated by the chains. Mark *et al.*[29] found that the distributions of the chain end-to-end distance are perturbed by the excluded volume effect. It causes the associated changes in the mechanical properties of the elastomer host matrix. The effects of nanoparticle size, loading, and shape on the mechanical properties of polymer nanocomposites have been investigated, and the rod-like nanoparticles have the greatest potential in improving the toughness of polymer nanocomposites.[30] Gersappe[31] found that the mobility of the nanofiller particle rather than its surface area controls its ability to dissipate energy, which can help improve the toughness of materials. Meanwhile, Jaber *et al.*[32] suggested that the mobility of the nanofiller particles helps in the construction and destruction of the networks of polymer nanocomposites under shear, and the fragility and the average length of stringlike motion are found to be dependent on the interfacial interaction between polymer and fillers and the filler concentration.[33]

On the basis of the aforementioned descriptions, although a large amount of research work has been devoted to improving the mechanical properties and exploring the mechanism of mechanical reinforcement, the underlying reasons are still not clearly revealed, especially for the nanorod filled rubber systems. In addition, it is very difficult to investigate the reinforcement mechanism clearly due to the very complicated filler dispersion state. Here we intend to study nanorod-filled elastomer networks to illustrate its reinforcement mechanism. In this work, we explore the factors influencing the stress–strain and molecular orientation behavior, by systematically tuning the polymer–nanorod interaction, aspect ratio of nanorod, nanorod functionalization, chemical couplings between polymer and nanorod, temperature and filler loading, which are always difficult to be realized quantitatively in the experiment.

2. Model and simulation methods

In the simulation, each idealized elastomer chain consists of thirty beads and the number of chains is 270. The nanorods consist of 3, 5, 8, 10 or 15 beads. We set the diameter of each bead to be σ and the mass to m. Here we used the truncated and shifted Lennard-Jones (LJ) interaction to model the polymer–polymer, polymer–nanorod and nanorod–nanorod interactions,[34] given by

$$U(r) = \begin{cases} 4\varepsilon\left[\left(\frac{\sigma}{r}\right)^{12} - \left(\frac{\sigma}{r}\right)^{6}\right] & r < r_{\text{cutoff}} \\ 0 & r \geq r_{\text{cutoff}} \end{cases} \quad (1)$$

where r_{cutoff} stands for the distance at which the interaction is truncated and shifted so that the potential is continuous at $r = r_{\text{cutoff}}$. The polymer–polymer interaction parameter and its cutoff distance are $\varepsilon_{\text{pp}} = 1.0$ and $r_{\text{pp}} = 2 \times 2^{1/6}$, and the nanorod–nanorod interaction parameter and its cutoff distance are set to $\varepsilon_{\text{nn}} = 1.0$ and $r_{\text{nn}} = 1.12$, respectively, while the polymer–nanorod interaction parameter ε_{np} and its cutoff distance r_{np} are changed to simulate different interfacial interaction strengths and ranges.

Additionally, the interaction between the adjacent bonded monomers including both polymer chains and nanorods is represented by a stiff finite extensible nonlinear elastic (FENE) potential:

$$V_{\text{FENE}} = -0.5kR_0^2 \ln\left[1 - \left(\frac{r}{R_0}\right)^2\right] \quad (2)$$

where $k = 30\frac{\varepsilon}{\sigma^2}$ and $R_0 = 1.5\sigma$. The rodlike character of the inclusions is enforced through an angle potential, given by

$$U_{\text{angle}} = K(1 + \cos(\theta)) \quad (3)$$

where θ is the bending angle formed by three consecutive rod beads and K is equal to 150.

Since it is not our aim to study a specific polymer, we used the LJ units where ε and σ are set to unity. It means that all calculated quantities are dimensionless. We initially constructed a relatively large system, and then the NPT ensemble was adopted with the temperature and pressure being fixed at $T^* = 1.0$ and $P^* = 0.0$, respectively, by using the Nose–Hoover temperature thermostat and pressure barostat.[35] It is noted that the number density of polymer beads ρ^* is more than 0.8 for all simulated systems, except for the case with $\varepsilon_{np} = 1.0$ and $r_{np} = 1.12\sigma$, in which the number density of polymer beads is $\rho^* \approx 0.65$. During the simulation, periodic boundary conditions are employed in all three directions. The velocity-Verlet algorithm is used to integrate the equations of motion, with a time step $\delta t = 0.001$, where the time is reduced by LJ time (τ).

We first add the cross-linking agents with diameter $D_{cl} = 0.5\sigma$ in the simulation box. After equilibration, permanent cross-links are formed by randomly selecting pairs of beads within a distance of 0.85σ of polymer monomers and cross-linking agents and tethering them together by using the modified FENE potential (eqn (4)). The number of cross-linking agents is 540.

The chemical bonding between polymer monomers and cross-linking agents is also modeled by the modified FENE potential as follows,

$$V_{FENE} = -0.5kR_0^2 \ln\left[1 - \left(\frac{r - R_{EV}}{R_0}\right)^2\right] \quad (4)$$

where $k = 30\frac{\varepsilon}{\sigma^2}$, $R_0 = 1.5\sigma$ and $R_{EV} = -0.25\sigma$.

Such structures are further equilibrated under the NVT ensemble with $T^* = 1.0$. After equilibration, the pure and nanofilled network systems are deformed by changing the box length to $L_0\alpha$ in one direction and to $L_0\alpha^{-1/2}$ in the other two directions so that the volume remains constant. In fact, we averaged the results in three directions. We set the strain rate $\dot{\varepsilon} = (L(t) - L)/L = 0.0327/\tau$.[36] The average stress τ in the tensile direction is obtained from the deviatoric part of the stress tensor $\tau = (1 + \mu)(-P_{\text{tensile direction}} + P) \cong 3(-P_{\text{tensile direction}} + P)/2$, where $P = \sum_i P_{ii}/3$ is the hydrostatic pressure. The parameter μ stands for Poisson's ratio. During the deformation process, rubber materials almost have no volume change and are incompressible, which make their Poisson's ratio equal to 0.5. This approach is introduced from the literature.[37–39] All MD runs are carried out by using the large scale atomic/molecular massively parallel simulator (LAMMPS) developed by Sandia National Laboratories.[40]

3. Results and discussion

3.1 Nanorod dispersion

Before studying the stress–strain behavior, firstly we characterized the filler dispersion state. The simulated temperature $T^* = 1.0$ in our simulation is well above the glass transition temperature of the pure polymer, which is around 0.5. The nanorod volume fraction is equal to 5.81% (the volume fraction is defined as the ratio of the volume of nanorods to the volume of the simulation box) and the aspect ratio of nanorod is 5. For a better understanding, we used (I)–(VII) to represent the following seven different systems. The r_{np} is 1.12σ for II (repulsive) and 2.5σ for III to VII (attractive). The chosen parameters were (I) the unfilled system, (II) $\varepsilon_{np} = 1.0$, (III) $\varepsilon_{np} = 1.0$, (IV) $\varepsilon_{np} = 2.0$, (V) $\varepsilon_{np} = 5.0$, (VI) $\varepsilon_{np} = 8.0$, and (VII) $\varepsilon_{np} = 12.0$. Here we used the inter-nanorod radial distribution function (RDF) to characterize its dispersion in Fig. 1(a). Obviously, for a strongly attractive interaction, $\varepsilon_{np} = 12.0$, there is a strong peak which exhibits a bifurcation in $g(r)$ at approximately $r = 2\sigma$, which means a ''bridging cluster'' of nanorods *via* one polymer layer as shown in Fig. S1(a) (ESI†). But the value of $g(r)$ at $r = 1\sigma$ is zero, indicating that there is no direct contact aggregation of nanorods. With the decrease of the interaction between polymers and nanorods, the low intensity peak indicates that nanorods are surrounded by a thermodynamically stable ''bound polymer layer''. At $\varepsilon_{np} = 2.0$, the system exhibits a best dispersion state. For purely repulsive polymer–nanorod interaction (*i.e.* Case II), all nanorods are almost in the direct contact aggregation state. For better illustration, the snapshots characterizing the nanorod dispersion state with three different interactions are shown in Fig. 1(b). The figure displays the best nanorod dispersion state at moderate polymer–nanorod interaction $\varepsilon_{np} = 2.0$. From the inter-agent radial distribution function $g(r)$ in Fig. S1(b) (ESI†), the cross-linking agents (purple spheres) also display the best dispersion at moderate polymer–nanorod interaction $\varepsilon_{np} = 2.0$.

Actually, we also explored the nanorod dispersion state in different nanorod volume fractions ($\varepsilon_{np} = 5.0$). The RDFs at different loadings are shown in Fig. 1(c). Obviously, the value of $g(r)$ at $r = 1\sigma$ is zero at low volume fraction (2.46%, 5.81%), indicating that there is no direct contact aggregation of nanorods. With the nanorod volume fraction increasing to 19.0%, a high peak appears at $r = 1\sigma$, suggesting the direct contact aggregation of nanorods. In general, with the increase of the nanorod volume loading, the dispersion of nanorods exhibits a trend from polymer bridge-induced clustering to partially direct contact aggregation.

3.2 Influence of polymer–nanorod interfacial strength

In this part, we solely investigated the effect of the polymer–nanorod interaction on the stress–strain behavior. We set the nanorod volume fraction equal to 5.81%, mainly considering that there is no direct contact aggregation of nanorods and the nanorod content is as high as possible in Fig. 1(c). First, we plotted the stress–strain curves of systems (I)–(VII) in Fig. 2(a). It can be seen that the stress–strain curves increase apparently with ε_{np}, which becomes more prominent at large deformation especially for large ε_{np}. By comparing the stress–strain curves between repulsive (II) and $\varepsilon_{np} = 1.0$(III) systems, we found that the interaction range between polymers and nanorods significantly influences the stress–strain behavior. To gain insight into the mechanical behavior, we plotted the stress–strain curves of systems $\varepsilon_{np} = 5.0$, 8.0, 12.0 at small deformation

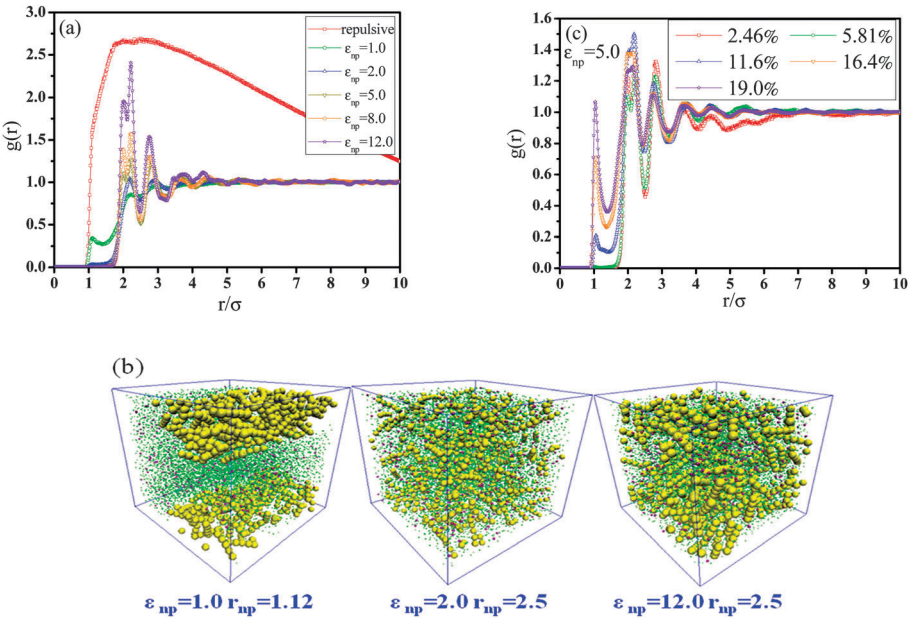

Fig. 1 (a) The radial distribution function $g(r)$ between nanorods for different polymer–nanorod interaction strengths and ranges. Note that the filler volume fraction is set to V = 5.81%. (b) The snapshots for three typical polymer–nanorod interfacial strengths. Note that the polymer chains are represented by green points to avoid obscuring the nanorods with yellow spheres, and the purple spheres represent the cross-linking agents. (c) The radial distribution function $g(r)$ for the filler volume fraction V = 2.46%, 5.81%, 11.6%, 16.4%, and 19.0% respectively.

($\Delta < 0.5$) as shown in the inset of Fig. 2(a). Unexpectedly, we observed that with an increase of the interaction strength, an obvious yield point appears. The point is around $\Delta \approx 0.12$ for ε_{np} = 5.0, 8.0, 12.0 although the yield point is not much obvious for ε_{np} = 5.0. To further explore the mechanism at the molecular level, we used the mean-square displacement (MSD) at time $t = 50\tau$ to characterize the mobility of polymer beads adjacent to the nanorod surface (within 1σ distance). For comparison, the corresponding MSD at time $t = 50\tau$ of polymer beads at the glassy state is also shown in Fig. 2(b), as indicated by the red line.

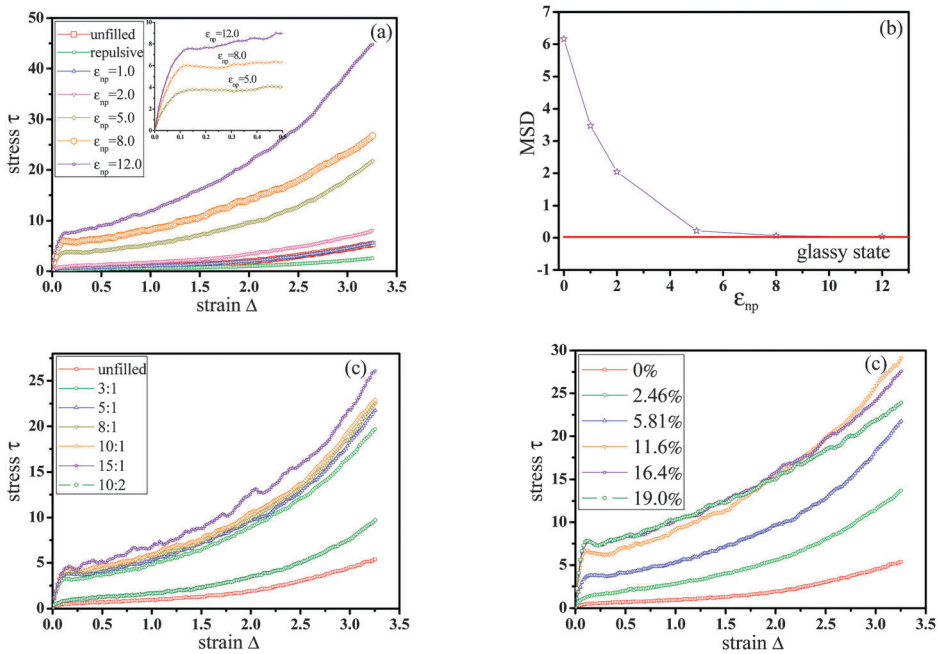

Fig. 2 Stress–strain curves (a) for systems filled with nanorods for different interaction strengths and ranges. The inset shows the plot of the stress–strain curves at small deformation $\Delta < 0.5$ for systems ε_{np} = 5.0, 8.0, 12.0. (b) The mean-square displacement of polymer beads in the vicinity of the nanorods as a function of interfacial strength, and for better comparison the corresponding glassy state is also added; (c) for systems filled with nanorods with different aspect ratios; and (d) for systems filled with different volume fractions.

Actually, the value of MSD decreases monotonically, indicating that the mobility of polymer beads in the vicinity of the nanorods decreases with the increase of ε_{np}. Meanwhile, when $\varepsilon_{np} > 5.0$, the MSD of interfacial polymer beads approaches one at the glassy state. Moreover, for the same polymer–nanorod interaction $\varepsilon_{np} = 12.0$ and at a lower volume fraction such as $V = 1.20\%$ and $V = 2.46\%$, no such yield point occurs (see Fig. S2 in the ESI†). Here we infer that the yield point may result from the interfacial layers with low mobility.

We interpret this yield phenomenon as follows: it has been shown that for $\varepsilon_{np} > 5.0$ the strongly "bridging clustering" of nanorods *via* one or two layers of polymer melts, and for high nanorod loading and strong polymer–nanorod interaction, it is possible to form a continuous nanorod network linked by polymer chains. In our opinion, the yield point could result from the breakage of the nanorod network structure in our simulated case. Meanwhile, to form a strong long-live polymer–nanorod network, high nanorod loading and strong polymer–nanorod interfacial strength are necessary.

Following this, we compared the stress–strain curves of unfilled, repulsive and $\varepsilon_{np} = 1.0$ systems. The mechanical properties of the repulsive system are lower than those of the unfilled system, without exhibiting a reinforcing effect. And the mechanical properties for $\varepsilon_{np} = 1.0$ are nearly the same as those of the unfilled system. However, the enhanced stress–strain behavior begins to occur for $\varepsilon_{np} = 2.0$. The results suggest that the reinforcing effect can be achieved only when the polymer–nanorod interaction is stronger than the polymer–polymer interaction.

3.3 Effect of the aspect ratio of the nanorod on the stress–strain behavior

In fact, in practical situations the nanorods always have various aspect ratios. In this section, we investigated the effect of the aspect ratio of nanorods on the stress–strain curves. Six different aspect ratios are chosen, which are defined as the ratio of length of the nanorod to diameter of the nanorod: (1) 3 : 1; (2) 5 : 1; (3) 8 : 1; (4) 10 : 1; (5) 15 : 1; (6) 10 : 2; the polymer–nanorod interaction strength is set to $\varepsilon_{np} = 5.0$, mainly considering that there is no direct contact aggregation of nanorods and the polymer–nanorod interface is relatively strong when the volume fraction of nanorod is also 5.81%. Nanorods have excellent dispersion as shown in Fig. S3 (ESI†). It is interesting to find that the nanorods exhibit a preference to be parallel to one direction for (5), while they all adopt a random orientation for other cases. From the stress–strain curves in Fig. 2(c), a gradually increased stress–strain behavior was observed when the aspect ratio of nanorod varies from (1) to (5), while a significant decrease in stress–strain curves was found for (6). The stress–strain curve was calculated only along the orientated direction of the nanorods for the aspect ratio of 15 : 1, and in this case the stress–strain behavior is greatly enhanced. For the same volume fraction, small-diameter nanorods give rise to greater surface area, allowing the maximization of interaction with the polymer matrix. The reason for this observation will be discussed later.

3.4 Effect of nanorod loading

To achieve good reinforcement, introducing high loading of nanorods into polymers is always necessary. Here we investigate the effect of the nanorod volume fraction on the stress–strain behavior. The polymer–nanorod interaction strength is set to $\varepsilon_{np} = 5.0$, the aspect ratio of nanorod is 5. The number of added nanorods $N = 425$, 1000, 2150, 3470, and 4360, corresponding to the nanorod volume fractions $V = 2.46\%$, 5.81%, 11.6%, 16.4%, and 19.0%, respectively. The stress–strain curves for different nanorod volume fractions are shown in Fig. 2(d).

From Fig. 2(d), we found that the stress gradually increases with the nanorod volume fraction at any strain and the difference in the stress at large strain becomes greater with the increase of the nanorod volume fraction, when the volume fraction is less than 11.6%. For instance, at strain $\Delta = 3.0$, the stress at the volume fraction of nanorods of 11.6% is approximately 4.7 times greater than that of the unfilled system. However, when the volume fraction of nanorods is greater than 11.6%, the stress at $\Delta = 3.0$ decreases with the increase of the volume fraction of nanorods. Actually, these results indicate that a higher nanorod volume fraction does harm to mechanical properties at large deformation. This underlying reason will also be illustrated later.

3.5 Effect of nanorod functionalization

Chemical functionalization of the nanorod surface is expected to maximize composite interfacial strength and achieve efficient interfacial stress transfer to the nanorod network. This method is especially effective for low interfacial strength. So we will discuss the effect of nanorod functionalization on the stress–strain behavior. The number of grafted agents and the length of grafted agents are represented by M and N, respectively.

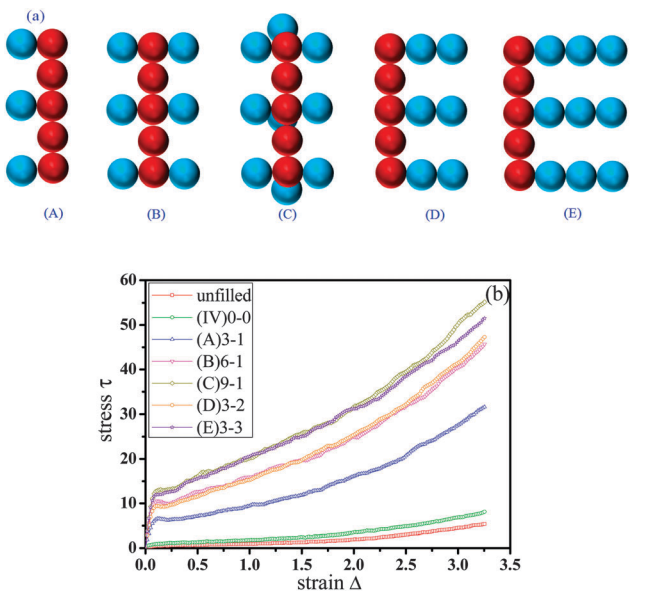

Fig. 3 (a) The snapshots of functionalized nanorods with three different lengths of grafted agents and three different number of grafted agents. The red spheres denote the nanorods. The blue spheres represent the surface modification agents. (b) The stress–strain curves for different functionalized nanorod filled systems.

The systems contain five cases (M-N) (A) 3-1; (B) 6-1; (C) 9-1; (D) 3-2; and (E) 3-3, as shown in Fig. 3(a). Here, the polymer–nanorod interaction is ε_{np} = 2.0 and the interaction between polymers and surface modification agents is ε_{sp} = 12.0. The nanorod–agent interaction is ε_{sn} = 1.0 and the agent–agent interaction is ε_{ss} = 1.0. The cutoff distance is always $r = 2.5\sigma$. The stress–strain curves in Fig. 3(b) exhibit a remarkable increase with the total number of surface modification agents, especially at large strain. For example, the stress of the filled system of 9-1(C) or 3-3(E) at strain $\Delta = 3$ is around 10 times greater than that of the unfilled system. When the total number of surface modification agents is equal, the difference in stress–strain curves seems to be tiny.

3.6 Effect of chemical couplings between polymers and nanorods

Covalent functionalization of nanorods is a very important factor for processing and application of nanorods, which can effectively improve the mechanical properties of the polymer–nanorod composites. In order to investigate the influence of chemical bonding on the stress–strain curves, here we used a bead as one coupling agent, linking a polymer bead with a nanorod bead. We used the FENE bond (eqn (2)) to model the chemical bonds. By forming different number of chemical coupling bonds between the polymers and the nanorods through coupling agents, we simulate different extents of chemical adhesion. Here we used N to denote the number of coupling agents, namely chemical bonds formed between polymers and nanorods. The stress–strain curves exhibit a remarkable increase with the number of chemical bonds, especially at large strain as shown in Fig. 4(a). For example, the stress of the filled systems with N = 600 at strain $\Delta = 3$ is approximately 25 times greater than that of the unfilled system. However, for the case of chemical bonds N = 600, when the simulation box is stretched along the y or z direction, some bonds of the simulated system will become broken before the box reaches the preset strain. These results imply that a certain degree of chemical bonds between polymers and nanorods is beneficial to improve the mechanical properties. However, excessive chemical bonds between polymers and nanorods will do harm to their mechanical properties, leading to the occurrence of fracture at decreased strain due to the significantly centralized stress. Our simulated results give evidence to support the experiment conclusion, *i.e.* the strong bonding is not necessary to enhance the mechanical properties of CNT-based materials.[20]

The approach used by Bokobza *et al.*[14,41] in the experiments is also adopted by us. We plotted the reduced stress $\tau^*(\tau^* = \tau/(\alpha^2 - \alpha^{-1}))$ against the reciprocal of the extension ratio $\alpha(\alpha = \Delta + 1)$, as suggested by the Mooney–Rivlin equation, given by

$$\tau^* = 2C_1 + 2C_2\alpha^{-1} \quad (5)$$

where $2C_1$ and $2C_2$ are constants independent of the extension ratio α. And the stress τ obtained in the simulation is the true stress. The result is shown in Fig. 4(b). It is very interesting to find that the filled systems with chemical bonds N = 400 and N = 600 display a clear upturn in the modulus at the high deformation and it is remarkable for the latter. The decrease in the modulus observed at low deformations can be attributed to the Payne effect. These Mooney–Rivlin plots qualitatively agree with the experimental results. The upturn in the modulus at large deformations is caused by the finite or limited chain extensibility limits, a further increase of the strain leads to the stiffer modes of deformation, bond length and bond angle changes. Meanwhile, this is accompanied by a significant decrease in the entropy of polymer chains with the corresponding increase in stress.

In addition, the role of chain scission becomes very important in the case of interfacial chemical couplings between polymers and nanorods, and we develop the following approach to consider the influence of the bond breakages with various number of interfacial chemical couplings N. For bonded beads A (its radius is r_A) and B (its radius is r_B), when the center-to-center distance between A and B is larger than $r_A + r_B + 0.3\sigma$, we assume that this bond is broken, which is the same with the literature.[42] The stress–strain curves are shown in Fig. 5(a). It is found that when the strain is smaller than 2.0, the stress–strain behavior is enhanced with N, while the stress reaches plateaus for all N when the strain is greater than 2.0, which can be explained by the fact that some bonds begin to quickly get broken at large strain. Meanwhile, we also characterize the change in the number of broken bonds as a function of the strain in Fig. 5(b),

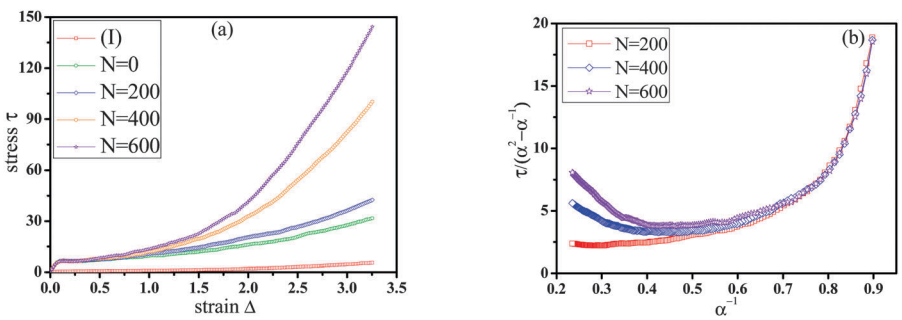

Fig. 4 (a) The stress–strain curves for filled systems with various number of chemical bonding N, the neat system is also included. N denotes the number of interfacial bonds. (b) Mooney–Rivlin plots of filled systems with different number of chemical bonds at V = 5.81%. Note that α denotes the extension ratio and is equal to $1 + \Delta$.

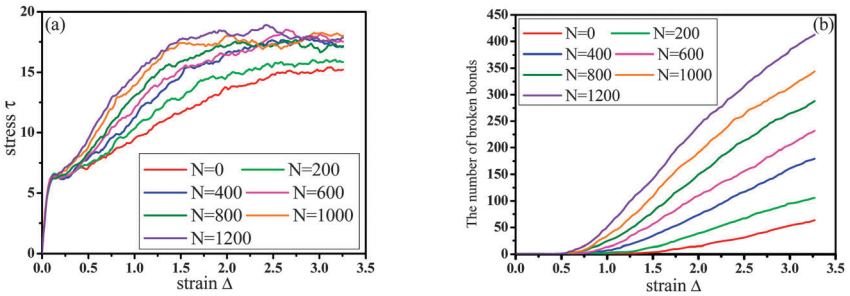

Fig. 5 (a) The stress–strain curves and (b) the number of broken bonds as a function of the strain for various number of interfacial chemical couplings N.

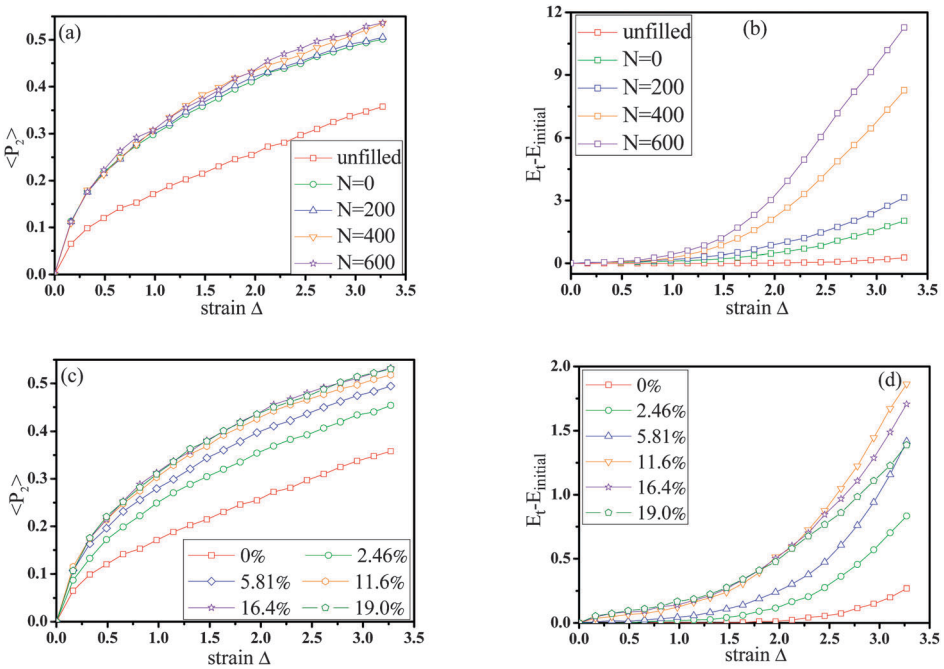

Fig. 6 The bond orientation $\langle P_2 \rangle$ with respect to the strain for systems (a) for filled systems with various numbers of chemical bonds N and (c) for different nanorod volume fraction filled systems. The change in bond energy $E_t - E_{initial}$ of the system with respect to the strain (b) for filled systems with various number of chemical bonding N and (d) for different nanorod volume fraction filled systems.

which shows that the number of broken bonds increases with the increase of the strain and N. It suggests that excessive interfacial chemical couplings with breakable bonds do not improve the mechanical properties.

In order to further examine the above phenomenon, we demonstrated the following approaches: the first method is to characterize the bond and nanorod orientations along the deformation direction with respect to the strain, and the second one is to examine the change in bond energy of the system with respect to the strain. First, we investigated the bond and nanorod orientations as a function of the strain for systems with chemical couplings between polymers and nanorods and different nanorod volume fractions as shown in Fig. 6(a) and (c). Here we used the second-order Legendre polynomials $\langle P_2 \rangle$ to characterize the bond and nanorod orientations as follows:

$$\langle P_2 \rangle = (3\langle \cos^2 \theta \rangle - 1)/2 \quad (6)$$

where θ denotes the angle between a given element (two adjoining beads in the chain or nanorods) and the reference direction, which in this work refers to the stretching direction. To calculate the orientation of polymer bonds or nanorods at any strain, we calculate the orientation of each polymer bond or each nanorod bond along the deformed direction, and add it up to get the average value divided by the total number of polymer bonds or nanorod bonds. Compared with that of the unfilled systems, a stronger bond orientation is observed for the filled systems at any equal strain. However, the bond orientation is almost the same, respectively, for the three systems with chemical couplings and three systems with V = 11.6%, 16.4% and 19.0%. In addition, the increased gradient of the bond orientation decreases gradually with the strain. These results support the viewpoint of the finite chain extensibility. At large deformation, chain deformation and segmental orientation caused by conformational rearrangements of chains slow down significantly, although the exerted force increases continuously.

Additionally, we plotted the change in the bond energy ($E_t - E_{initial}$) as a function of the strain, respectively, in Fig. 6(b) and (d). From the figure, the bond energy of the unfilled system remains nearly unchanged during the deformation process. While for the other systems the bond energy of the system increases greatly with the number of the chemical couplings during the deformation process. This increasing trend becomes particularly obvious at large deformation. It is noted that in the case of the filled system with chemical couplings $N = 200$, the increase in bond energy mainly comes from polymer chains, rather than other chemical bonds between polymers and nanorods. Since at the strain $\Delta = 3.27$, the change in bond energy of the filled system with chemical bonds $N = 200$ is equal to $E_{100\tau} - E_{initial} = 3.05$, while the change becomes $E_{100\tau} - E_{initial} = 2.77$, when we turn off the chemical bonds except the polymer–polymer bonds and cross-linking bonds. In general, it indicates that the finite chain extensibility surely occurs at large deformation, especially for the filled system with enough chemical couplings between polymers and nanorods. Meanwhile, according to our simulation, the upturn of the modulus at large deformation, as shown in Fig. 4(b), can only be seen for the filled system with enough chemical couplings in the interface.

Next we come back to the issue of why the reinforcing efficiency declines after the nanorod volume fraction goes beyond $V = 11.6\%$. By examining the change in the bond energy with respect to the strain, we can give a reasonable interpretation in Fig. 6(d). For the nanorod loading $V < 11.6\%$, the increase in the extent of the bond energy of the system becomes much greater with the increase of nanorod volume loading, while for $V > 11.6\%$, the increase in slope declines. For better illustration, in Fig. 7 we presented the change in the bond energy at $\Delta = 3.27$ derived from Fig. 6(d), which exhibits a maximum value at around $V = 11.6\%$. The analysis shows that too high nanorod loading will hinder the development of the finite chain extensibility, leading to less contribution of the bond energy to the stress–strain behavior. Therefore, the reinforcing efficiency declines at $V = 16.4\%$ and 19.0%. This can also be understood by the fact that if the nanorod loading is too high, there is not enough space for the extension of the bond lengths at large deformation. At the same time, the optimal volume fraction of 11.6% corresponds to that the dispersion state of nanorods varies from no direct contact aggregation to direct contact aggregation. So we can present evidence that the finite chain extensibility surely comes into effect at large deformation and enough strong chemical bonding between polymers and nanorods will lead to an upturn of the modulus at large deformation in the Mooney–Rivlin plots. Especially, as shown in Fig. 1(c), the peak at around 2σ corresponds to bridging configurations, namely first nanorod–nanorod neighbors surrounded by only one polymer bead, which form a polymer–nanorod network. The bridge peak reaches a maximum at 11.6% loading, namely, maximizing the polymer–nanorod network. The stronger the polymer–nanorod network, the better the mechanical property. The existence of an optimal loading for the mechanical reinforcement had also been found for the case of spherical fillers, and the nanorods are the most efficient for mechanical reinforcement compared to spherical and sheet-like fillers.[30]

3.7 Temperature effect

In this section, we investigated the effect of temperature on the stress–strain curves, because polymer chains exhibit completely different flexibilities, especially above or below its glass transition temperature. Following the literature,[43] the equilibrated states at the glassy state are obtained by cooling the equilibrated configurations at high temperatures, namely by reducing the dimensionless temperature by 0.02 every 500 000 MD time steps. Here we chose three filler volume fractions $V = 0$, 5.81% and 11.6%, which were simulated at $T = 1.0$ for a rubbery state and at $T = 0.2$ for a glassy state. The interaction strength between the matrix and the filler is $\varepsilon_{np} = 5.0$ and the cutoff distance is 2.5σ. From Fig. 8, an increase in the stress–strain curves is found by adding nanorods into the glassy polymer matrix (stress ($V = 11.6\%$)/stress ($V = 0\%$) = 1.9 at $\Delta = 3$), while a more significantly enhanced stress–strain behavior is observed when introducing nanorods into the rubbery matrix (stress ($V = 11.6\%$)/stress ($V = 0\%$) = 5.7 at $\Delta = 3$). Meanwhile the incorporated nanorods would also bear some stress. In fact, for the glassy and rubbery polymer matrices by incorporating nanorod particles, the difference in reinforcement efficiency is consistent with the practical application of polymer nanocomposites. This point is also illustrated in the literature[44] and here we can infer that the more significant reinforcement can be obtained in the rubber

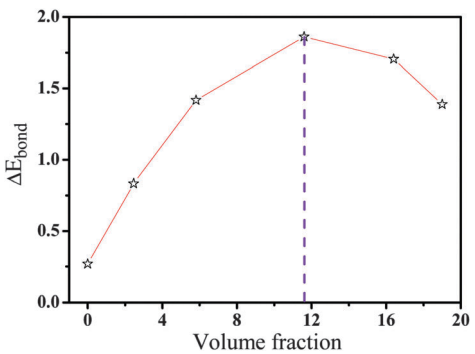

Fig. 7 The change in the bond energy ΔE_{bond} as a function of the filler volume loading calculated from Fig. 6(d).

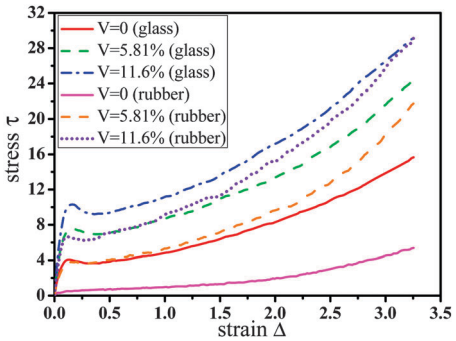

Fig. 8 Stress–strain curves for nanorod filled polymer systems (glassy and rubbery) with different filler volume fractions above and below the glass transition temperature.

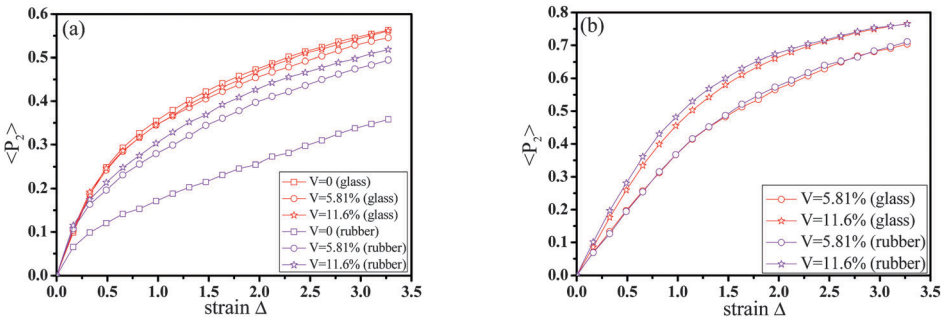

Fig. 9 (a) The bond orientation $\langle P_2 \rangle$ and (b) the nanorod orientation $\langle P_2 \rangle$ of the glassy and rubber systems with different filler volume fractions.

polymer matrices than the glassy polymer matrices by incorporating nanorod particles. As shown in Fig. 9, for the glassy systems, the bond orientation nearly does not change with the increase of the nanorod loading, while the nanorod orientation continuously increases. So we believe that the increase of reinforcement only comes from the increase of the nanorod orientation for the glassy systems. However, both the bond and nanorod orientations increase for the rubbery systems. It can be rationalized by the fact that in the glassy state, the bond orientation does not increase which is hindered by its low mobility, making it very hard to slip on the filler surface. This leads to a more effective enhancement of mechanical properties for rubbery systems rather than for glassy systems. Some further discussion is addressed in the ESI.†

4. Conclusions

To uncover the mechanical reinforcement mechanism of nanorod filled polymers, we investigate the stress–strain behavior by tuning the polymer–nanorod interaction, aspect ratio of nanorods, nanorod functionalization, chemical couplings and nanorod loading. Firstly the nanorod dispersion state was characterized in detail, and a better nanorod dispersion state was observed at intermediate polymer–nanorod interfacial strength and low nanorod loading. Meanwhile, the simulation results indicate that there exists an optimum nanorod filler volume fraction for rubber reinforcement. The increase of the interfacial strength improves the mechanical properties, and a yielding point occurs at strong interfacial strength and high filler volume fraction, which are attributed to the breakage of a strong nanorod network *via* polymer chains. The mechanical strength displayed great improvement for nanorods with longer length and smaller diameter. The chemical functionalization of nanorods can achieve efficient interfacial stress transfer from the polymer matrix to the nanorods. A significant increase in the stress–strain curve occurs, and an upturn in the modulus at large deformation in the Mooney–Rivlin plot with strong enough chemical couplings is found, which is mainly caused by the finite chain extensibility at large deformation. However, excessive chemical couplings between polymer and nanorods are detrimental to mechanical properties, which could lead to stress-concentration centers. The reinforcement is realized by the alignment and orientation of both polymer chains and nanorods, and the limited extensibility of chains at large deformation. With stronger polymer–nanorod network, the modulus will improve more, which is reflected by the change in van der Waals pairwise energy (VDWL). Additionally, we also examined the bond and nanorod orientation in the filled glassy and rubbery polymer systems, explaining why rubbery systems exhibit more significantly enhanced reinforcement than glassy systems.

Acknowledgements

This work was supported by NSF of China (91334203, 21274011), The National 863 Program (2009AA03Z338), National Scientific Research Funding (ZZ1304), the Foundation for Innovative Research Groups of the NSF of China (51221002), and National Basic Research Program (2011CB706900), "Chemical Grid Project" and Excellent Talents Funding of BUCT.

References

1 M. Moniruzzaman and K. I. Winey, *Macromolecules*, 2006, **39**, 5194–5205.
2 T. Kuilla, S. Bhadra, D. H. Yao, N. H. Kim, S. Bose and J. H. Lee, *Prog. Polym. Sci.*, 2010, **35**, 1350–1375.
3 R. Sengupta, M. Bhattacharya, S. Bandyopadhyay and A. K. Bhowmick, *Prog. Polym. Sci.*, 2011, **36**, 638–670.
4 H. M. Smallwood, *J. Appl. Phys.*, 1944, **15**, 758–766.
5 O. Gold and E. Guth, *Phys. Rev.*, 1938, **53**, 322–325.
6 E. Guth, *J. Appl. Phys.*, 1945, **16**, 20–25.
7 G. Huber and T. A. Vilgis, *Macromolecules*, 2002, **35**, 9204–9210.
8 J. Berriot, H. Montes, F. Lequeux, D. Long and P. Sotta, *Macromolecules*, 2002, **35**, 9756–9762.
9 G. J. Papakonstantopoulos, M. Doxastakis, P. F. Nealey, J. L. Barrat and J. J. de Pablo, *Phys. Rev. E: Stat. Phys., Plasmas, Fluids, Relat. Interdiscip. Top.*, 2007, **75**, 031803.
10 M. Vacatello, *Macromolecules*, 2001, **34**, 1946–1952.
11 V. M. Litvinov and P. A. W. Steeman, *Macromolecules*, 1999, **32**, 8476–8490.
12 H. Luo, M. Kluppel and H. Schneider, *Macromolecules*, 2004, **37**, 8000–8009.
13 S. Merabia, P. Sotta and D. R. Long, *Macromolecules*, 2008, **41**, 8252–8266.
14 L. Bokobza and B. Erman, *Macromolecules*, 2000, **33**, 8858–8864.

15 W. F. Reichert, D. Goritz and E. J. Duschl, *Polymer*, 1993, **34**, 1216–1221.
16 Y. Hou, J. Tang, H. B. Zhang, C. Qian, Y. Y. Feng and J. Liu, *ACS Nano*, 2009, **3**, 1057–1062.
17 J. N. Coleman, M. Cadek, R. Blake, V. Nicolosi, K. P. Ryan, C. Belton, A. Fonseca, J. B. Nagy, Y. K. Gun'ko and W. J. Blau, *Adv. Funct. Mater.*, 2004, **14**, 791–798.
18 J. N. Coleman, U. Khan and Y. K. Gun'ko, *Adv. Mater.*, 2006, **18**, 689–706.
19 F. Deng, M. Ito, T. Noguchi, L. F. Wang, H. Ueki, K. Niihara, Y. A. Kim, M. Endo and Q. S. Zheng, *ACS Nano*, 2011, **5**, 3858–3866.
20 M. Naraghi, G. H. Bratzel, T. Filleter, Z. An, X. Wei, S. T. Nguyen, M. J. Buehler and H. D. Espinosa, *Adv. Funct. Mater.*, 2012, **23**, 1883–1892.
21 L. Xie, F. Xu, F. Qiu, H. B. Lu and Y. L. Yang, *Macromolecules*, 2007, **40**, 3296–3305.
22 G. L. Hwang, Y. T. Shieh and K. C. Hwang, *Adv. Funct. Mater.*, 2004, **14**, 487–491.
23 J. Zhu, H. Q. Peng, F. Rodriguez-Macias, J. L. Margrave, V. N. Khabashesku, A. M. Imam, K. Lozano and E. V. Barrera, *Adv. Funct. Mater.*, 2004, **14**, 643–648.
24 D. Blond, V. Barron, M. Ruether, K. P. Ryan, W. J. Blau and J. N. Coleman, *Adv. Funct. Mater.*, 2006, **16**, 1608–1614.
25 T. A. Vilgis, *Polymer*, 2005, **46**, 4223–4229.
26 G. N. Toepperwein, R. A. Riggleman and J. J. de Pablo, *Macromolecules*, 2012, **45**, 543–554.
27 S. T. Knauert, J. F. Douglas and F. W. Starr, *J. Polym. Sci., Part B: Polym. Phys.*, 2007, **45**, 1882–1897.
28 M. S. Ozmusul, C. R. Picu, S. S. Sternstein and S. K. Kumar, *Macromolecules*, 2005, **38**, 4495–4500.
29 J. E. Mark, R. Abou-Hussein, T. Z. Sen and A. Kloczkowski, *Polymer*, 2005, **46**, 8894–8904.
30 A. Kutvonen, G. Rossi, S. R. Puisto, N. K. J. Rostedt and T. Ala-Nissila, *J. Chem. Phys.*, 2012, **137**, 214901.
31 D. Gersappe, *Phys. Rev. Lett.*, 2002, **89**, 058301.
32 E. Jaber, H. B. Luo, W. T. Li and D. Gersappe, *Soft Matter*, 2011, **7**, 3852–3860.
33 F. W. Starr and J. F. Douglas, *Phys. Rev. Lett.*, 2011, **106**, 115705.
34 J. S. Smith, D. Bedrov and G. D. Smith, *Compos. Sci. Technol.*, 2003, **63**, 1599–1605.
35 J. Liu, D. P. Cao and L. Q. Zhang, *J. Phys. Chem. C*, 2008, **112**, 6653–6661.
36 J. Gao and J. H. Weiner, *J. Chem. Phys.*, 1995, **103**, 1614–1620.
37 D. R. Rottach, J. G. Curro, J. Budzien, G. S. Grest, C. Svaneborg and R. Everaers, *Macromolecules*, 2006, **39**, 5521–5530.
38 D. R. Rottach, J. G. Curro, J. Budzien, G. S. Grest, C. Svaneborg and R. Everaers, *Macromolecules*, 2007, **40**, 131–139.
39 D. R. Rottach, J. G. Curro, G. S. Grest and A. P. Thompson, *Macromolecules*, 2004, **37**, 5468–5473.
40 S. Plimpton, *J. Comput. Phys.*, 1995, **117**, 1–19.
41 L. Bokobza, *Polymer*, 2001, **42**, 5415–5423.
42 M. Panico, S. Narayanan and L. C. Brinson, *Model. Simul. Mater. Sci. Eng.*, 2010, **18**, 055005.
43 K. Binder, J. Baschnagel and W. Paul, *Prog. Polym. Sci.*, 2003, **28**, 115–172.
44 Z. H. Wang, J. Liu, S. Z. Wu, W. C. Wang and L. Q. Zhang, *Phys. Chem. Chem. Phys.*, 2010, **12**, 3014–3030.

